Supplemental Material:
A Physically-Based BSDF for Modeling the Appearance of Paper

Marios Papas, Krystle de Mesa, and Henrik Wann Jensen

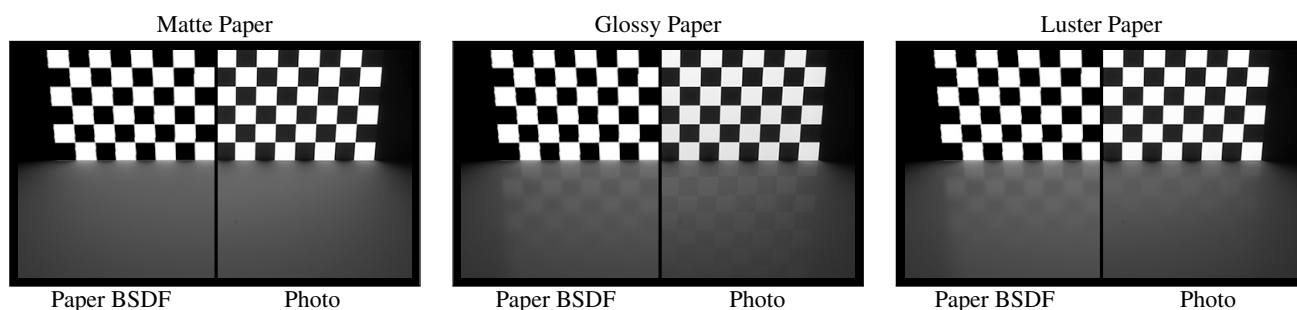University of California, San Diego

Figure 1: *Comparisons between a photograph (right side) and our Paper BSDF (left side). The scene is of an illuminated checkerboard pattern with matte (left), glossy (middle), and luster (right) papers placed in front of it.*

Abstract

This supplemental material provides additional figures and derivations that complement our paper. The main paper includes indicative examples from the full set of plots contained in this document. We present graphical plots that detail how each of the Paper BSDF's components contribute to closely replicating our BSDF measurements for paper. We also offer comparison plots for Lambertian/Rough Glass BSDF and an unmodified multi-layer BSSRDF to show how these models are not good solutions for fully capturing the features of paper.

1. Light scatter distance in paper

In Figure 2, we plot two horizontal scanlines from a linear HDR macro photo with equal lengths of $2mm$. Matte paper and brushed aluminum samples were illuminated from normal incidence while a blocker casted a hard shadow vertical to the plotted scanlines.

Since no direct light arrives at the shadowed region, what we capture as reflected light from that region is mainly due to two reasons: subsurface scattering and measurement errors. Since metal has no subsurface scattering, we would ideally expect to see an immediate transition from the maximum value to the lowest value when using a point light. In Figure

2, we see a transition from 5% to 95% of the maximum pixel value for metal in $0.2mm$. This can be attributed to the fact that our light source is a small area light, to focus errors and inter-reflections. In red, we show the shadow edge plot for matte paper. The distance from 5% to 95% of the maximum pixel value for paper is $0.72mm$. This shows that at small scale there is some measurable light scatter distance in paper.

For rendering applications where the camera resolution and light features are less than a millimeter, our Paper BSDF will not apply the proper spatial blurring due to subsurface scattering. Please note that this does not imply any limitations for

our paper measurements since all locations that contribute to our measurement region are uniformly illuminated.
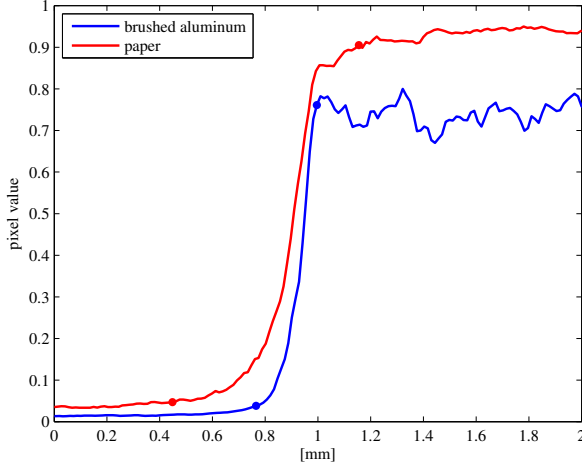

Figure 2: Shadow edge plots for matte paper (red) and brushed aluminum (blue).

2. Integrating $R(r)$

$R(r)$ is defined by [DJ05] to represent the reflectance for $2n+1$ dipoles. This is equal to the sum of each dipole's contribution:

$$R(||x_i - x_o||) = R(r) \tag{1}$$

$$= \sum_{i=-n}^{n} \frac{\alpha' z_{r,i}(1 + \sigma_{tr} d_{r,i}) e^{-\sigma_{tr} d_{r,i}}}{4\pi d_{r,i}^3} - \frac{\alpha' z_{v,i}(1 + \sigma_{tr} d_{v,i}) e^{-\sigma_{tr} d_{v,i}}}{4\pi d_{v,i}^3}.$$

For each dipole, $d_{r,i} = \sqrt{r^2 + z_{r,i}^2}$ and $d_{v,i} = \sqrt{r^2 + z_{v,i}^2}$ represents the distances from x_i to the real and virtual point light sources. Similarly, $z_{r,i} = 2i(d + z_b(0) + z_b(d)) + l$ and $z_{v,i} = 2i(d + z_b(0) + z_b(d)) - l - 2z_b(0)$ are the distances from x_o to the real and virtual point light sources. For the front ($z = 0$) and back ($z = d$) surface, the fluence extinction boundary distances are defined as $z_b(z) = 2A(z)D$, with $D = \frac{1}{3\sigma_t'}$ as the diffusion constant. $A(z)$, the extrapolation distance, is defined as $A(0) = \frac{1 + \rho_{in}(0)(\eta_f, m_f)}{1 - \rho_{in}(\eta_f, m_f)}$ and $A(d) = \frac{1 + \rho_{in}(d)(\eta_b, m_b)}{1 - \rho_{in}(\eta_b, m_b)}$ for the front and back surface, respectively. Diffuse reflection factor $\rho_{in}(z)$ corresponds to the BSDF integral over all incident and outgoing directions within the hemisphere defined by the negative surface normal. Other terms used in our multiple scattering equations are specified in Table 1.

By using R_d, we effectively remove 1 sampling dimension from the BSSRDF, thus converting its reflectance to a 3D BRDF and allowing for more dense samples. We thus integrate $R(r)$ in the following manner:

$$R_d = 2\pi \int_0^\infty R(r) r dr \tag{2}$$

$$= 2\pi \int_0^\infty \sum_{i=-n}^{n} \left(\frac{\alpha' z_{r,i}(1 + \sigma_{tr} d_{r,i}) e^{-\sigma_{tr} d_{r,i}}}{4\pi d_{r,i}^3} - \frac{\alpha' z_{v,i}(1 + \sigma_{tr} d_{v,i}) e^{-\sigma_{tr} d_{v,i}}}{4\pi d_{v,i}^3} \right) r dr$$

$$= 2\pi \sum_{i=-n}^{n} \int_0^\infty \left(\frac{\alpha' z_{r,i}(1 + \sigma_{tr} d_{r,i}) e^{-\sigma_{tr} d_{r,i}}}{4\pi d_{r,i}^3} - \frac{\alpha' z_{v,i}(1 + \sigma_{tr} d_{v,i}) e^{-\sigma_{tr} d_{v,i}}}{4\pi d_{v,i}^3} \right) r dr$$

$$= -\frac{\alpha'}{2} \sum_{i=-n}^{n} \left| \frac{z_{r,i} e^{-\sigma_{tr}\sqrt{z_{r,i}^2 + r^2}}}{\sqrt{z_{r,i}^2 + r^2}} - \frac{z_{v,i} e^{-\sigma_{tr}\sqrt{z_{v,i}^2 + r^2}}}{\sqrt{z_{v,i}^2 + r^2}} \right|_0^\infty$$

$$= \frac{\alpha'}{2} \sum_{i=-n}^{n} \left(sign(z_{r,i}) e^{-\sigma_{tr}|z_{r,i}|} - sign(z_{v,i}) e^{-\sigma_{tr}|z_{v,i}|} \right).$$

Symbol	Description
$\alpha' = \frac{\sigma_s'}{\sigma_t'}$	Reduced albedo
$\sigma_s' = \left(1 - (w_b g_b + w_f g_f)\right)\sigma_s$	Reduced scatter coefficient
$\sigma_{tr} = \sqrt{(3\sigma_a \sigma_t')}$	Effective transport coefficient
$sign(a)$	1 if $a \geq 0$ and -1 if $a < 0$

Table 1: Multiple Scattering Nomenclature

3. Integrating $T(r)$

The amount of light that enters the front surface of the material at x_i and exits from the back surface at x_o is

$$T(||x_i - x_o||) = T(r) \tag{3}$$

$$= \sum_{i=-n}^{n} \frac{\alpha'(d - z_{r,i})(1 + \sigma_{tr} d_{r,i}) e^{-\sigma_{tr} d_{r,i}}}{4\pi d_{r,i}^3} - \frac{\alpha'(d - z_{v,i})(1 + \sigma_{tr} d_{v,i}) e^{-\sigma_{tr} d_{v,i}}}{4\pi d_{v,i}^3},$$

where $d_{r,i} = \sqrt{(d - z_{r,i})^2 + r^2}$ and $d_{v,i} = \sqrt{(d - z_{v,i})^2 + r^2}$ are the distances of x_o from the real and the virtual light sources, respectively. The other terms are defined in Section 2 and Table 1. Integrating $T(r)$ similarly to $R(r)$ in Sec-

tion 2, we get the following result:

$$T_d = 2\pi \int_0^\infty T(r) r dr \qquad (4)$$

$$= 2\pi \int_0^\infty \sum_{i=-n}^n \left(\frac{\alpha'(d-z_{r,i})(1+\sigma_{tr}d_{r,i})e^{-\sigma_{tr}d_{r,i}}}{4\pi d_{r,i}^3} - \right.$$
$$\left. \frac{\alpha'(d-z_{v,i})(1+\sigma_{tr}d_{v,i})e^{-\sigma_{tr}d_{v,i}}}{4\pi d_{v,i}^3} \right) r dr$$

$$= 2\pi \sum_{i=-n}^n \int_0^\infty \left(\frac{\alpha'(d-z_{r,i})(1+\sigma_{tr}d_{r,i})e^{-\sigma_{tr}d_{r,i}}}{4\pi d_{r,i}^3} - \right.$$
$$\left. \frac{\alpha'(d-z_{v,i})(1+\sigma_{tr}d_{v,i})e^{-\sigma_{tr}d_{v,i}}}{4\pi d_{v,i}^3} \right) r dr$$

$$= -\frac{\alpha'}{2} \sum_{i=-n}^n \left| \frac{(d-z_{r,i})e^{-\sigma_{tr}\sqrt{(d-z_{r,i})^2+r^2}}}{\sqrt{(d-z_{r,i})^2+r^2}} - \right.$$
$$\left. \frac{(d-z_{v,i})e^{-\sigma_{tr}\sqrt{(d-z_{v,i})^2+r^2}}}{\sqrt{(d-z_{v,i})^2+r^2}} \right|_0^\infty$$

$$= \frac{\alpha'}{2} \sum_{i=-n}^n \left(sign(d-z_{r,i})e^{-\sigma_{tr}|d-z_{r,i}|} - \right.$$
$$\left. sign(d-z_{v,i})e^{-\sigma_{tr}|d-z_{v,i}|} \right).$$

4. $\vec{P}_{\text{valid}}$ for the Paper BSDF

Parameter	[min,max]	Description
η_f/η_b	(1,5)	Relative index of refraction of the front/back surface
m_f/m_b	$[\varepsilon,\pi/2]$	Front surface roughness
σ_a	$[0,\infty]$	Absorption events per mm
σ_s	$[0,\infty]$	Scattering events per mm
g_b/g_f	[-1,1]	Mean cosine of back/forward scattered light
w_b	[0,1]	Weight for backscattered light
d	$[\varepsilon,\infty]$	Paper thickness in mm

Table 2: Valid ranges of the Paper BSDF parameters used as bounds during fitting. Please note that the paper thickness d was actually measured.

5. Paper BSDF Fitted Plots

Figure 3 presents graphical plots of our Paper BSDF fitted against in-plane BSDF measurements for paper. Below we detail how our model accounts for each paper's distinguishing features.

Matte Paper. To capture the grazing angle sheen in matte paper, we use a combination of single scattering and surface reflection. Microfacet models can also explain grazing angle sheen, but we found that adding forward single scattering to the equation provided a much better fit instead. Retroreflection is modeled with a backward single scattering component, and for scattered light attenuation, we used our surface BTDF integration method, ρ_{dt}, as described in the main paper. To estimate matte paper's roughness, we found that the GGx distribution function provides a much better fit for these surfaces than Beckmann distribution.

Luster and Glossy Photo Paper. Both luster and glossy photo paper have an off-specular peak near the reflection direction due to varied levels of gloss on the front surface of the paper; this provides an added surface smoothness that is absent in matte paper. We estimate this smoothness with the Beckmann distribution function. As with matte paper, the back surface of these photo papers exhibit the same roughness and multiple scattered light attenuation, thus we treat the back surface in the same manner by using our ρ_{dt} integration method of the BTDF with GGx distribution. We also found that the slightly stronger retroreflection recovered is due to limitations of the analytic Henyey-Greenstein phase function. As Gkioulekkas et al. [GZB*13] also suggest, real world phase functions can be very different from currently available analytic models and can also have a strong impact on perceived appearance [GXZ*13].

6. Lambertian with Rough Glass BRDF Fitted Plots

Figure 4 showcases the Lambertian and Rough Glass BRDF fitted against our BRDF measurements for luster and glossy paper. The plots show the Lambertian model unable to adequately fit against the BRDF measurements.

7. Reduced multi-layer BSDF Fitted Plots

Figure 5 was generated by integrating the reduced multi-layer BSDF without using our attenuation term, $Att(\vec{i}, \eta, m)$, introduced in the main paper. Although the matte paper BRDF appears to have an adequate fit with the multi-layer model, the flat shape of the multiple scattered light in these BRDF plots imply that the front surface is smooth, which is incorrect. This inaccurate estimation of multiple scattered light is also shown in the BTDF plots.

References

[DJ05] DONNER C., JENSEN H. W.: Light diffusion in multi-layered translucent materials. *ACM Trans. Graph. 24*, 3 (July 2005), 1032–1039. 2

[GXZ*13] GKIOULEKAS I., XIAO B., ZHAO S., ADELSON E. H., ZICKLER T., BALA K.: Understanding the role of phase function in translucent appearance. *ACM Trans. Graph. 32*, 5 (Oct. 2013), 147:1–147:19. 3

[GZB*13] GKIOULEKAS I., ZHAO S., BALA K., ZICKLER T., LEVIN A.: Inverse volume rendering with material dictionaries. *ACM Trans. Graph. 32*, 6 (Nov. 2013), 162:1–162:13. 3
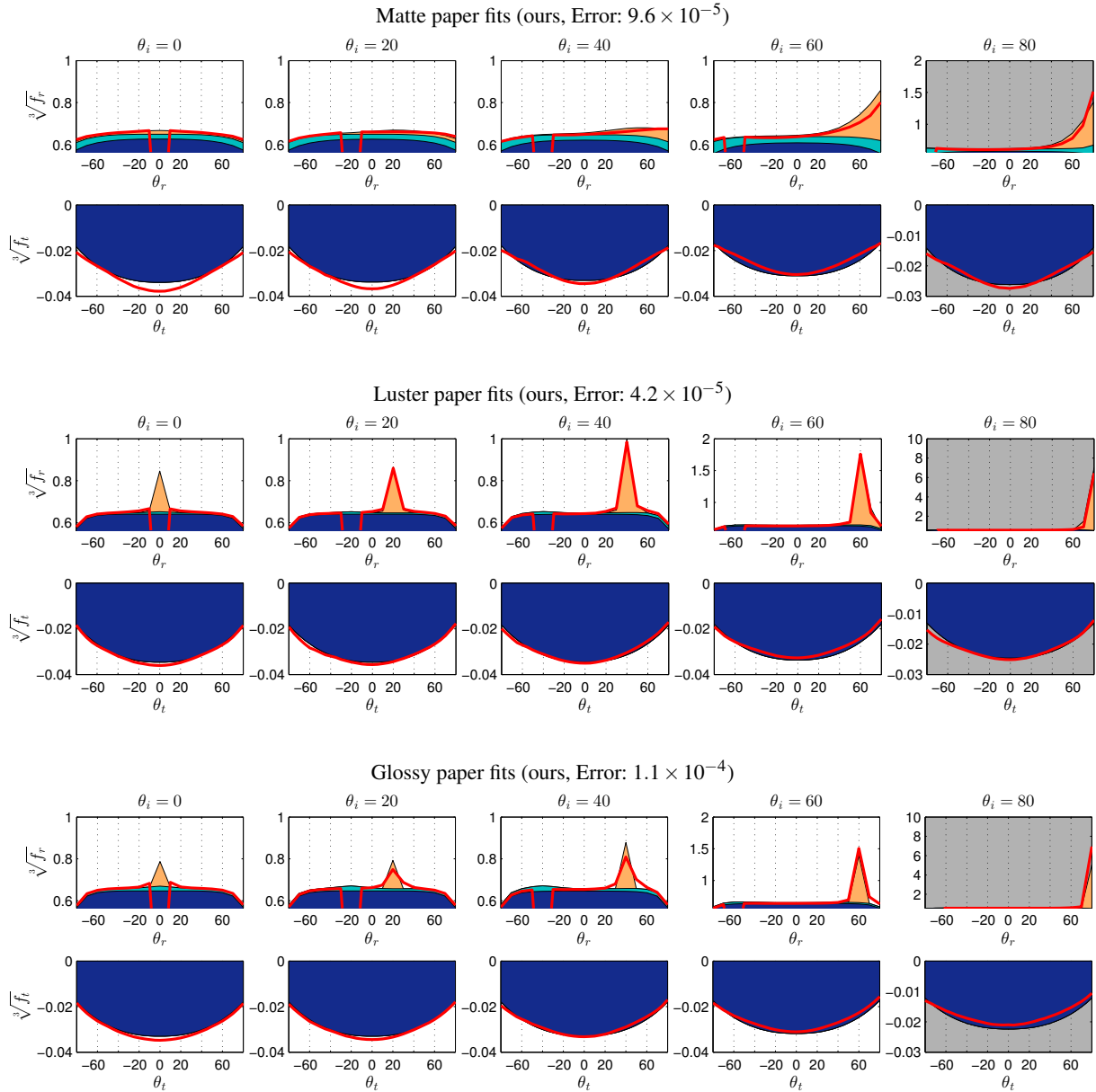
Figure 3: **Paper BSDF fitting results:** Matte (top), luster (middle), and glossy paper in-plane fitting results with measured values (red line) and our model broken down into its separate components: surface reflection (orange), single scattering (cyan), and multiple scattering (blue). The extrapolated comparison of the measurements and the optimal model fit are shown with a gray background.
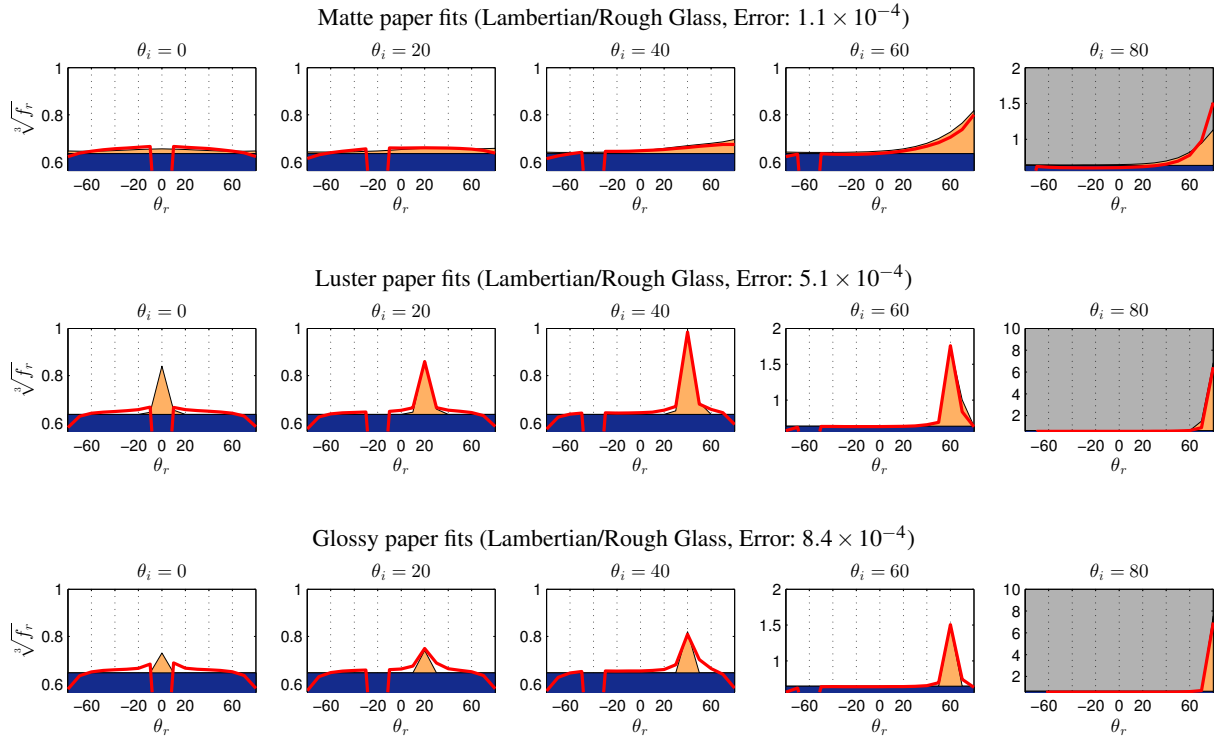
Figure 4: **Lambertian/Rough Glass BRDF fitting results:** Matte (top), luster (middle), and glossy (bottom) paper in-plane fitting results with measured values (red line), Lambertian (blue), and the rough glass BRDF (orange). The extrapolated comparison of the measurements and the optimal model fit are shown with a gray background.
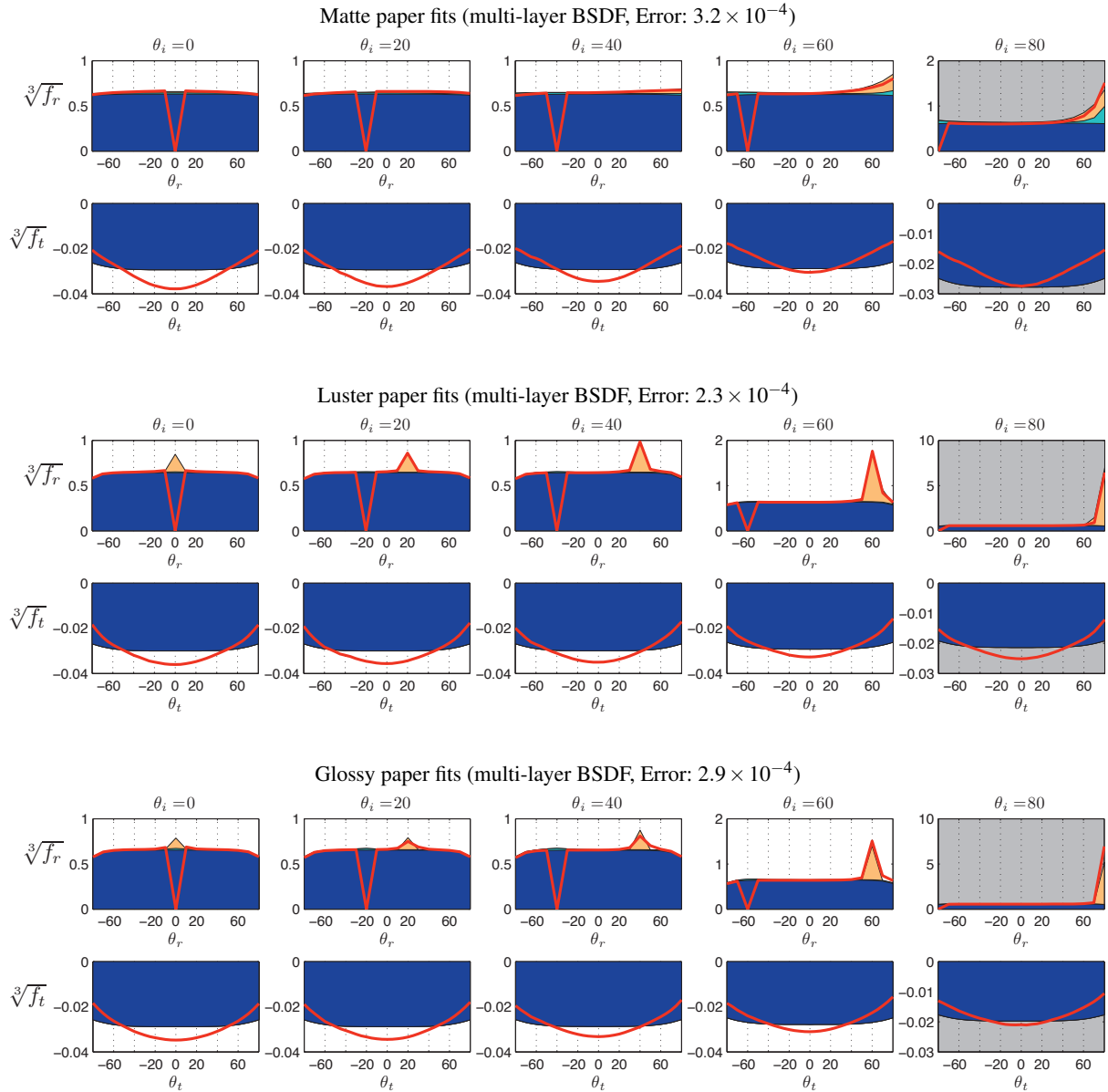
Figure 5: **Reduced multi-layer BSDF fitting results:** Matte (top), luster (middle), and glossy (bottom) paper in-plane fitting results with measured values (red line), surface reflection (orange), single scattering (cyan), and a single layer from the reduced multi-layer BSDF (blue). The extrapolated comparison of the measurements and the optimal model fit are shown with a gray background.